Title

FLUID FLOW MODEL OF THE CERRO PRIETO GEOTHERMAL FIELD BASED ON WELL LOG INTERPRETATION

Authors

Halfman, S.E.
Lippmann, M.J.
Zelwer, R.
et al.

Publication Date

1982-10-01

CONF-8208107--6

LBL-14898
CERRO PRIETO-26

MEXICAN-AMERICAN COOPERATIVE PROGRAM AT THE CERRO PRIETO GEOTHERMAL FIELD

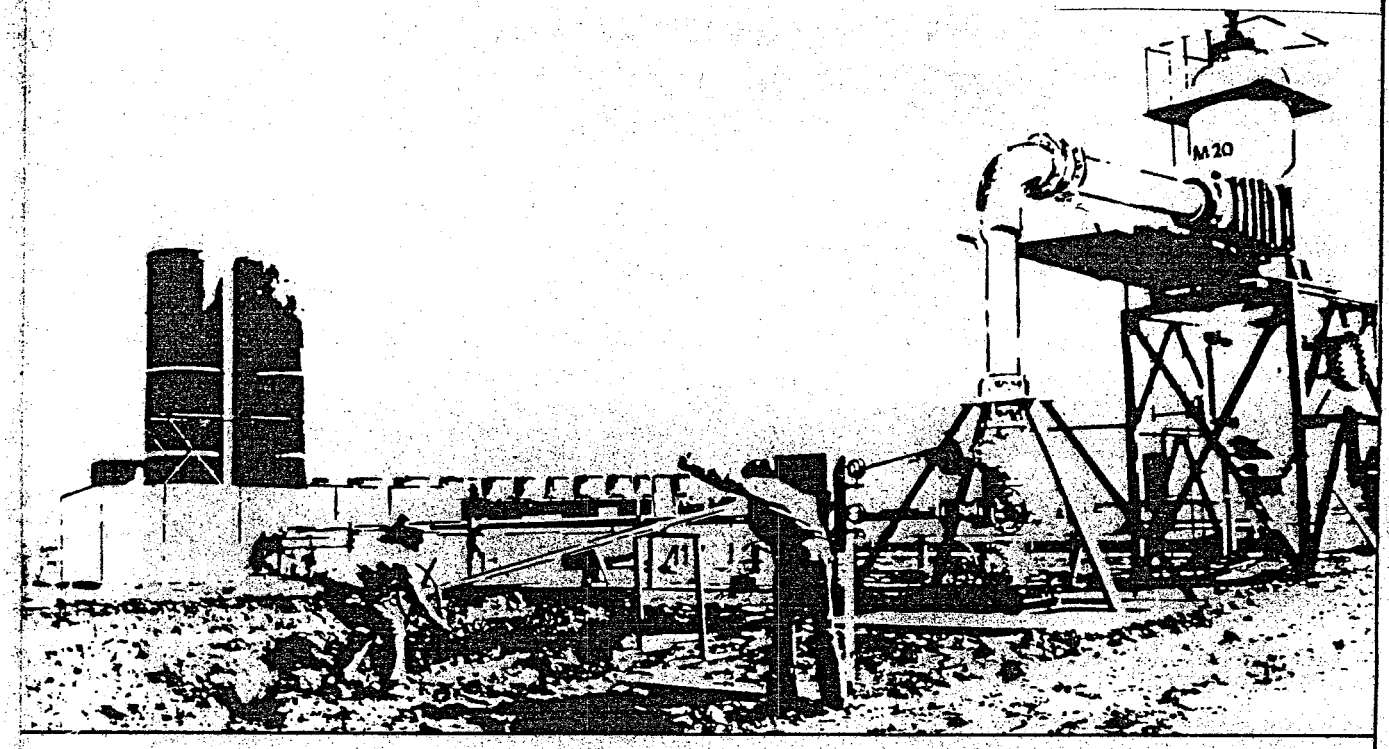

Presented at the Fourth Symposium on the Cerro Prieto Geothermal Field, Guadalajara, Mexico, August 10-12, 1982

FLUID FLOW MODEL OF THE CERRO PRIETO GEOTHERMAL FIELD BASED ON WELL-LOG INTERPRETATION

S. E. Halfman, M. J. Lippmann, R. Zelwer, and J. H. Howard

October 1982

A Joint Project of

COMISION FEDERAL DE ELECTRICIDAD
México

DEPARTMENT OF ENERGY
Division of Geothermal Energy
United States of America

Coordinated by

Coordinadora Ejecutiva
de Cerro Prieto
Apdo. Postal No. 3-636
Mexicali, Bja. Cfa., México
and P. O. Box 248
Calexico, Ca. 92231

Lawrence Berkeley Laboratory
Earth Sciences Division
University of California
Berkeley, California 94720
Operating for the U.S. Department of Energy under Contract Number
DE-AC03-76SF00098

DISCLAIMER

Presented at the 4th Symposium on the Cerro Prieto Geothermal Field, Guadalajara, Mexico, August 10-12, 1982.

LBL-14898
CP-26

FLUID FLOW MODEL OF THE CERRO PRIETO GEOTHERMAL FIELD BASED ON WELL LOG INTERPRETATION

by

S.E. Halfman[1], M.J. Lippmann[1], R. Zelwer[1], and J.H. Howard[2]

[1]Earth Sciences Division
Lawrence Berkeley Laboratory, University of California
Berkeley, California 94720

[2]Cities Service Company, Tulsa, Oklahoma 74102

October 1982

This work was supported by the Assistant Secretary of Conservation and Renewable Energy, Office of Renewable Technology, Division of Geothermal and Hydropower Technologies of the U.S. Department of Energy under Contract No. DE-AC03-76SF00098.

FLUID FLOW MODEL OF THE CERRO PRIETO GEOTHERMAL FIELD BASED ON WELL LOG INTERPRETATION

S.E. Halfman[1], M.J. Lippmann[1], R. Zelwer[1] and J.H. Howard[2]
[1]Earth Sciences Division
Lawrence Berkeley Laboratory, University of California
Berkeley, California 94720
[2]Cities Service Company, Tulsa, Oklahoma 74102

ABSTRACT

The subsurface geology of the Cerro Prieto geothermal field was analyzed using geophysical and lithologic logs. The distribution of permeable and relatively impermeable units and the location of faults are shown in a geologic model of the system. By incorporating well completion data and downhole temperature profiles into the geologic model, it was possible to determine the direction of geothermal fluid flow and the role of subsurface geologic features that control this movement.

INTRODUCTION

To accurately assess the future potential of the Cerro Prieto field, it is important to determine the circulation pattern of the geothermal fluids in the subsurface. A hydrogeologic model of the geothermal system has been developed on the basis of data from over 90 wells that have been drilled in the field (Figure 1). The results obtained from this model can be used in reservoir engineering studies of the field. The methodology used in this study should be applicable to other geothermal systems situated in a sedimentary environment, such as those of the Salton Trough.

Hot geothermal fluid at Cerro Prieto is found mainly in the nearly circular area shown in Figure 2. In the eastern part of the field (near wells M-109, T-328, T-348, and M-115), fluid is produced at depths of about 7000 to 9500 ft.; in the western region (near wells M-26, M-34, and M-15A), at depths of about 3400 to 5000 ft. Along the western edge of the field (near well M-6), some geothermal fluid leaks to the surface. In general, this indicates that fluid flows from great depths in the east, gradually rising as it moves westward, where some escapes to the surface (e.g., Mercado, 1968; Elders et al., 1981).

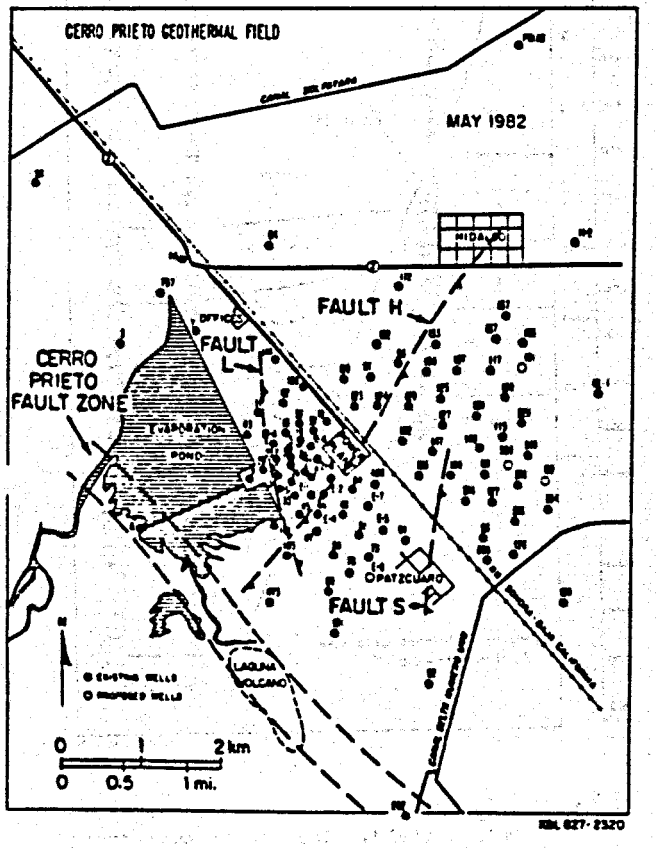

Figure 1. Location of wells and faults at Cerro Prieto.

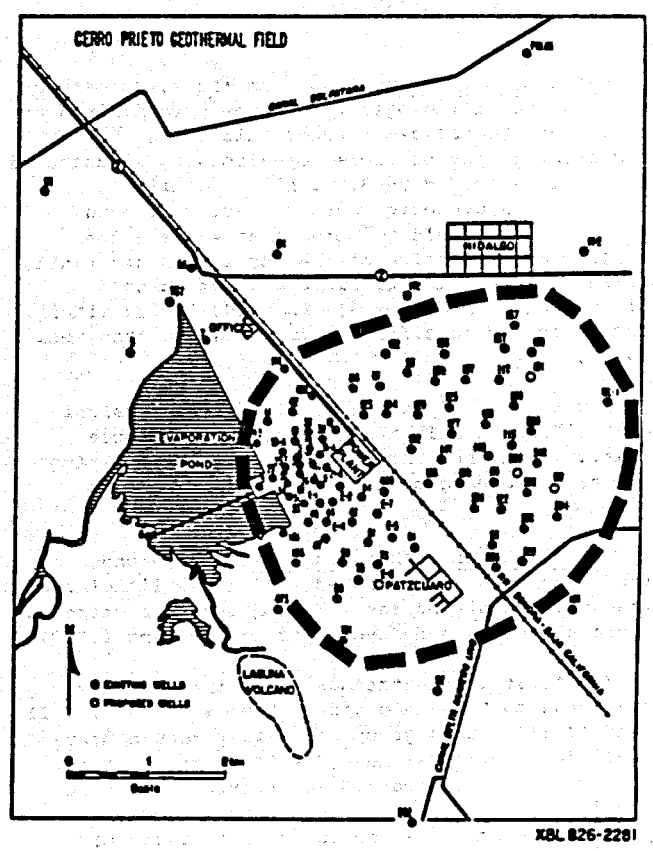

Figure 2. Location of the bulk of the hot geothermal fluid.

METHODOLOGY

A geologic model of the Cerro Prieto field was first constructed based on geophysical and lithological well logs. Downhole temperature profiles and well production interval data were then incorporated into the geologic model to develop a geothermal fluid flow model that would determine the actual fluid flow paths. The fluid flow model was then used to identify the lithologic and structural features that control the movement of the geothermal fluid.

Geologic Model

The following types of well logs were used to develop the geologic model of Cerro Prieto: gamma-ray (GR), spontaneous potential (SP), laterolog-8 (LL8), medium induction (ILM), deep induction (ILD), short normal resistivity (RSN), long normal resistivity (RLN), compensated formation density gamma-gamma (RHOB), dipmeter (DIP), and lithologic (LITH) logs. The logs were digitized at 1-ft intervals, stored in a computer, and displayed graphically using a 2-ft sampling interval. For correlation purposes, each log (except LITH and DIP logs) was reduced, so that a log for a well 10,000 ft deep was reduced from 500 in. to approximately 13 in.

Two methods were used to define the stratigraphy. In the first method, formations were defined on basis of their lithology. In the second method, a simplified version of Lyons and van de Kamp's (1980) approach was used in which lithofacies were defined according to thickness of sand (or shale) beds and well log characteristics.

Definition of formations. In the first method, seven distinct lithologic formations were defined by analysis of the above-mentioned well logs. The basic stratigraphy of these formations is illustrated using GR logs in Figure 3. Table 1 details the geologic and hydrologic characteristics of each formation. It should be noted that whereas the overall characteristics of the formations are easily correlated across the field (e.g., Formation 3, as illustrated in Figure 3), individual beds within a formation may be difficult to correlate from well to well.

Faults were identified on the basis of significant differences in the depth of correlatable formations and from the identification of "missing" sections of some formations.

Definition of lithofacies. In the second method, the beds were grouped into three lithofacies units on the basis of the well log analysis criteria (Figure 4) followed by Lyons and van de Kamp (1980).

The first is a sandstone group that roughly corresponds to Lyons and van de Kamp's units I, I-II, II and II-III. This group consists predominantly of well-defined sandstones (20-150 ft thick) interbedded with shales (most 20-30 ft thick, but some 50-70 ft thick). The well logs have a blocky appearance, which is a common characteristic of stacked channels, eolian deposits, and delta front sands or channel overbank sands on a deltaic plain.

The second is a sandy-shale group that generally corresponds to Lyons and van de Kamp's unit III and consists of roughly equal amounts of sandstones and shales. The sandstones can be as much as 30 ft thick and commonly have transitional bases, which can be characteristic of delta front and distributary overbank deposits in a delta plain. Some beds in this group were difficult to categorize on the reduced log curves. Beds that did not fit into the first or third groups were assigned to this one. Consequently, it became characterized as a transitional group between the first and third.

The third is a shale group that corresponds to Lyons and van de Kamp's units III-IV, IV, IV-V, and V. This group includes thinly bedded sandstones/shales (many less than 10 ft thick) as well as thicker shales (± 40 ft thick) with some thin sandstone intercalations. The well logs show features typical of distal overbank, delta plain, swamp, coastal bay, and lagoonal deposits.

After assigning the beds to the different lithofacies groups, lithofacies cross-sections were constructed incorporating the faults identified by the first method.

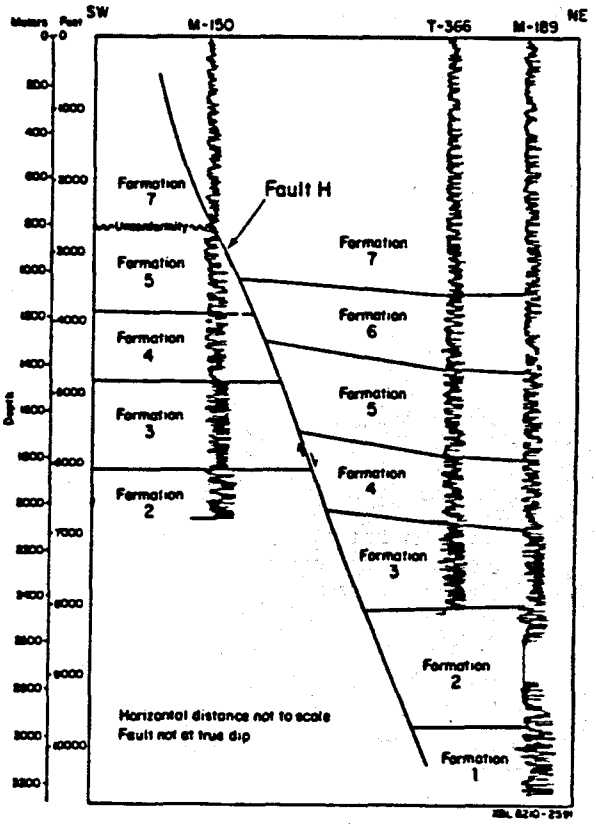

Figure 3. Simplified stratigraphy of the Cerro Prieto field. The traces correspond to gamma-ray logs.

Table 1. General geologic and hydrologic characteristics of the formations identified in the field (Figure 3).

Formation	General Geologic Characteristics	Hydrologic Characteristics
7	Lower section primarily a shale unit overlain by a progressively sandier unit, in turn overlain by another shale unit.	Relatively unaffected by heat of geothermal fluids.
6	Alternating sandstone and shale beds with sandstones varying in thickness from 10 to 300 ft or more.	Relatively unaffected by heat of geothermal fluids.
5	Alternating sandstone and shale beds averaging 30 to 60 ft in thickness.	Uppermost shale beds act as a local cap rock to the α reservoir west of the railroad tracks.
4	Shales up to 100 ft thick; some thin sandstone beds; some interbedded sandstones and shales of varying thicknesses; may be difficult to distinguish from Formation 3 when GR logs are not available.	Contains part of the α reservoir, which is found mainly west of the railroad tracks and northwest of Fault H.
3	Thinly bedded sandstones and shales (sandstones are often less than 10 ft thick).	Acts as a local cap rock to the β reservoir in most regions of the field; in some areas west of the railroad tracks, it contains part of the α reservoir in its upper 500 ft.
2	GR has a blocky appearance; sands sometimes as thick as 70 ft; lower section has some thinly bedded sandstones and shales.	β reservoir contained in the upper section, where thicker sands are present.
1	Alternating sandstone and shale beds of varying thicknesses.	Below β reservoir

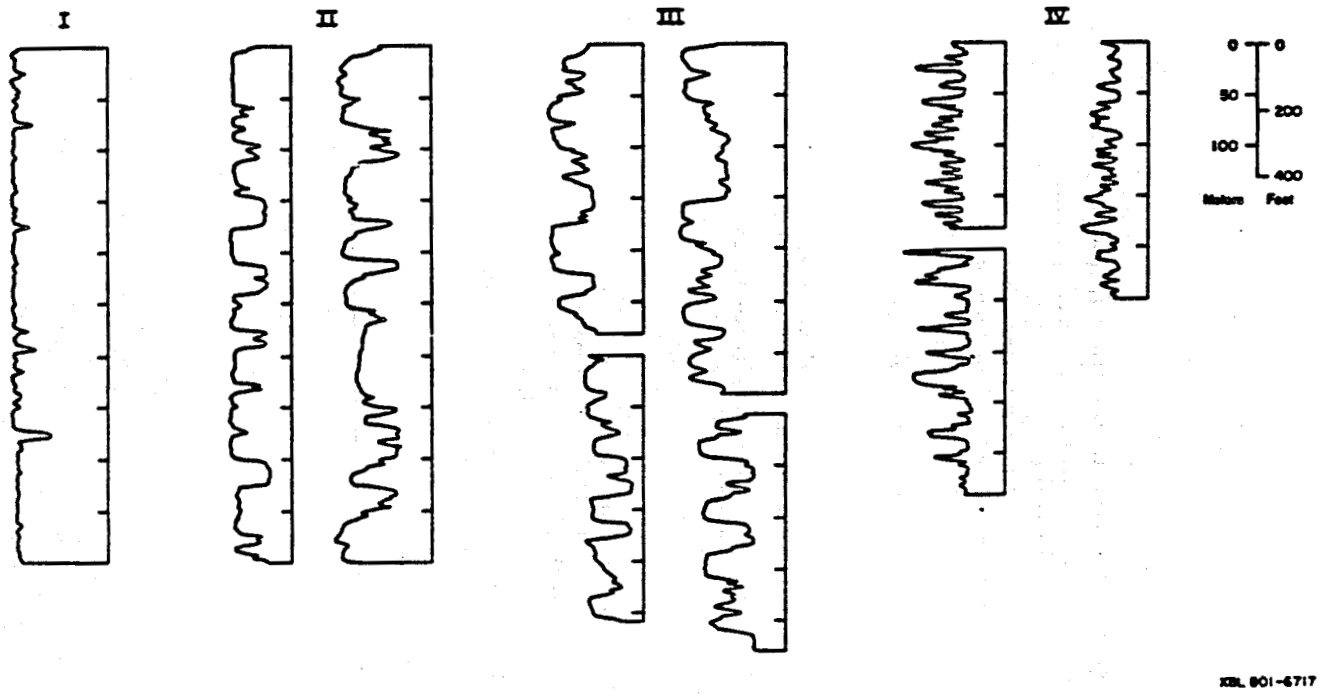

Figure 4. Examples of the lithofacies classes based on the SP curve. (After Lyons and van de Kamp, 1980)

Geothermal Fluid Flow Model

To construct the geothermal fluid flow model, downhole temperature profiles and production intervals were superimposed on the lithofacies cross-sections. The temperature profiles identified the depths at which temperatures of commercial interest were found (generally > 280°C), while the well production intervals indicated zones of higher permeability from which hot fluids are produced.

The interpretation of these geological and reservoir engineering data allowed us to determine the flow direction and paths of the geothermal fluids and the geologic features controlling their movement through the field, as described below.

GEOLOGIC MODEL

Formation Cross-Sections

Five cross-sections were developed (locations shown in Figure 5) and are given in Figures 6A-E, showing the configuration of the seven lithologic formations identified in this study.

Cross-section A-A' (Figure 6A) illustrates a typical correlation of formations across the field, including the location of faults and producing intervals in the wells. The deep wells east of the railroad tracks (RR between wells M-10 and M-123) have been drilled into Formation 2. The B (or β) reservoir (Prian, 1981; Sánchez and de la Peña, 1981) is located in this formation. The reservoir temperature ranges from 300°C to 350°C.

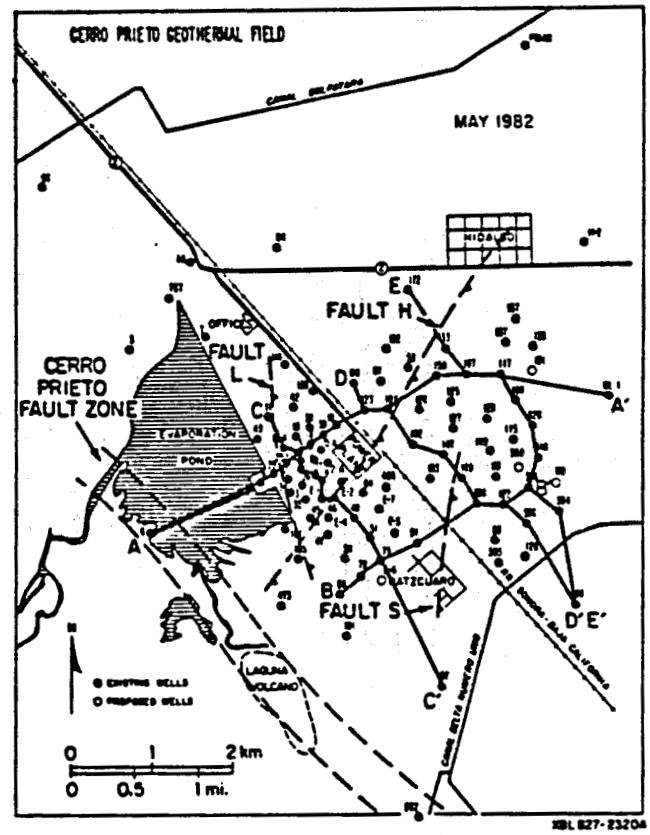

Figure 5. Location of cross-sections.

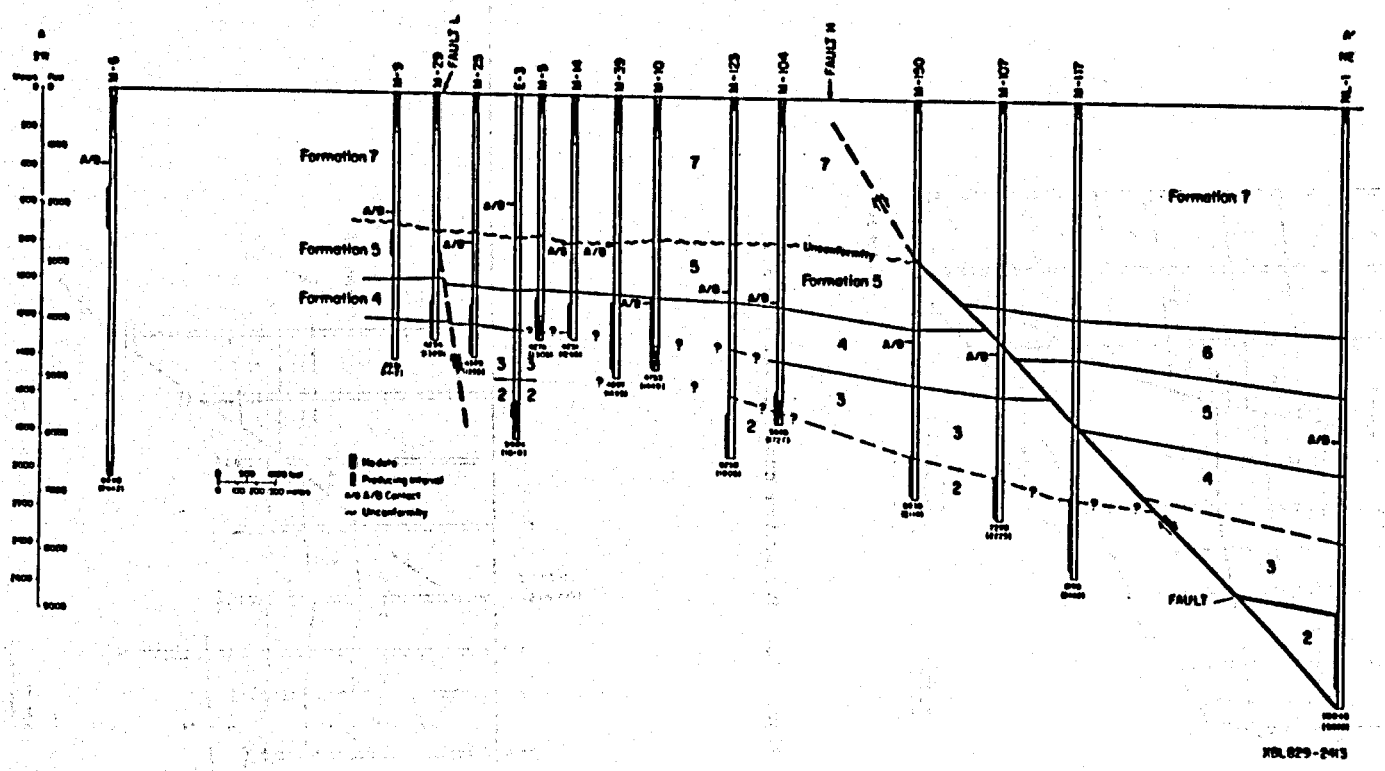

Figure 6A. Formation cross-section A-A'.

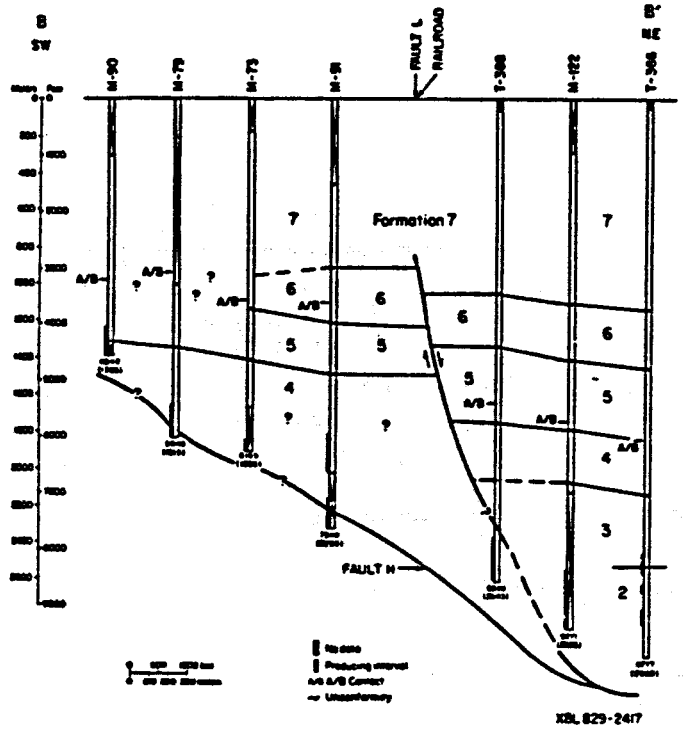

Figure 6B. Formation cross-section B-B'.

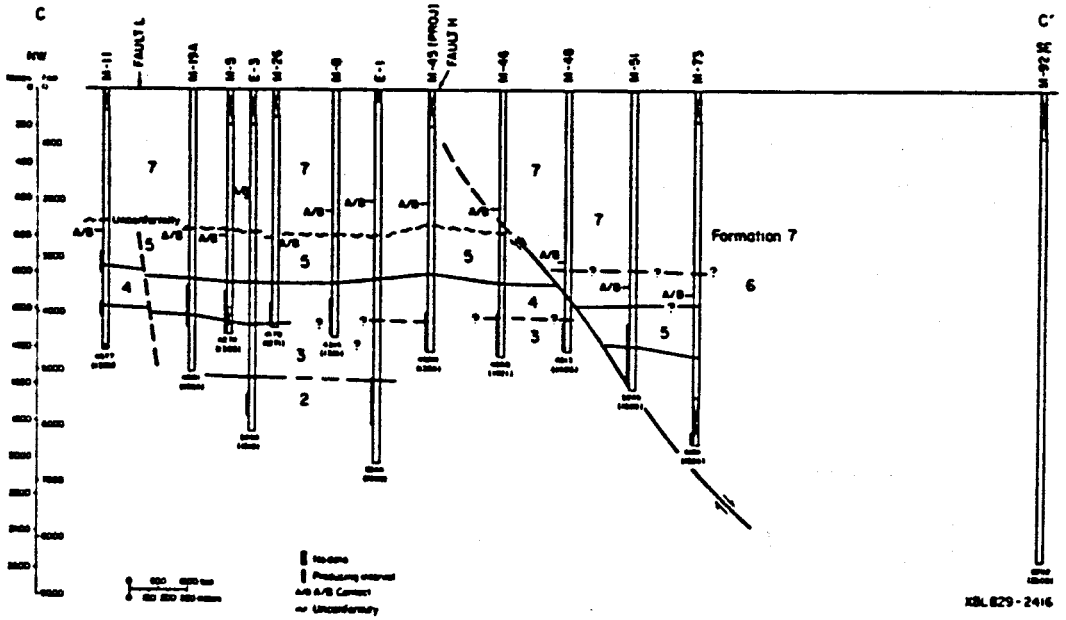

Figure 6C. Formation cross-section C-C'.

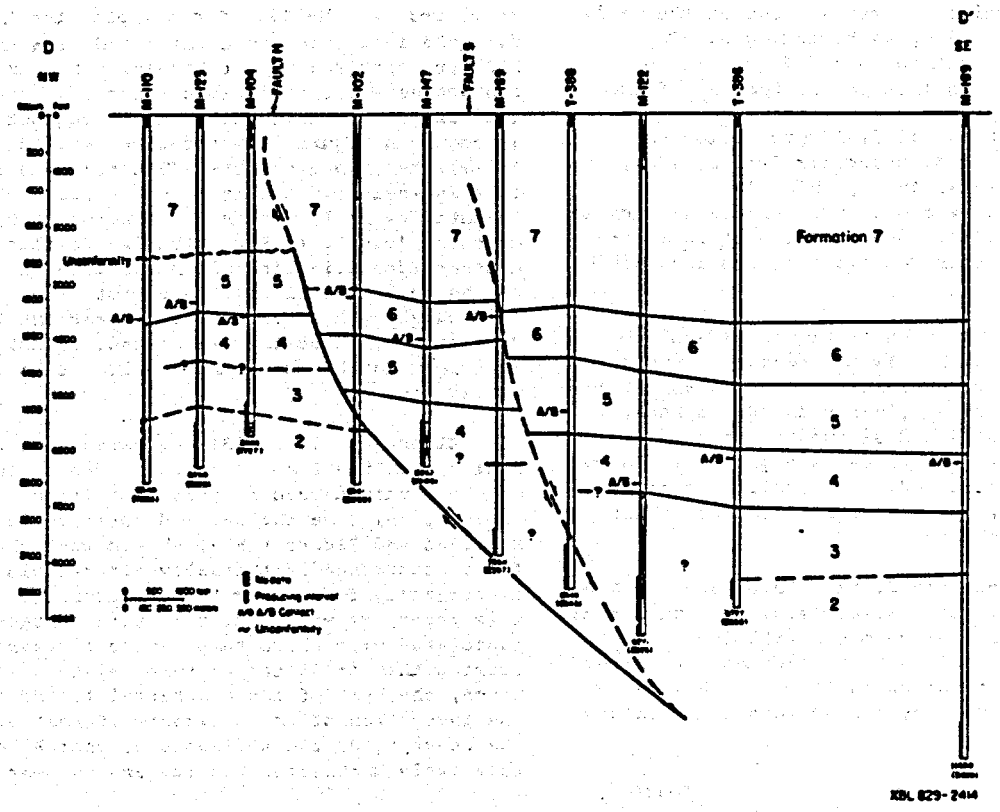

Figure 6D. Formation cross-section D-D'.

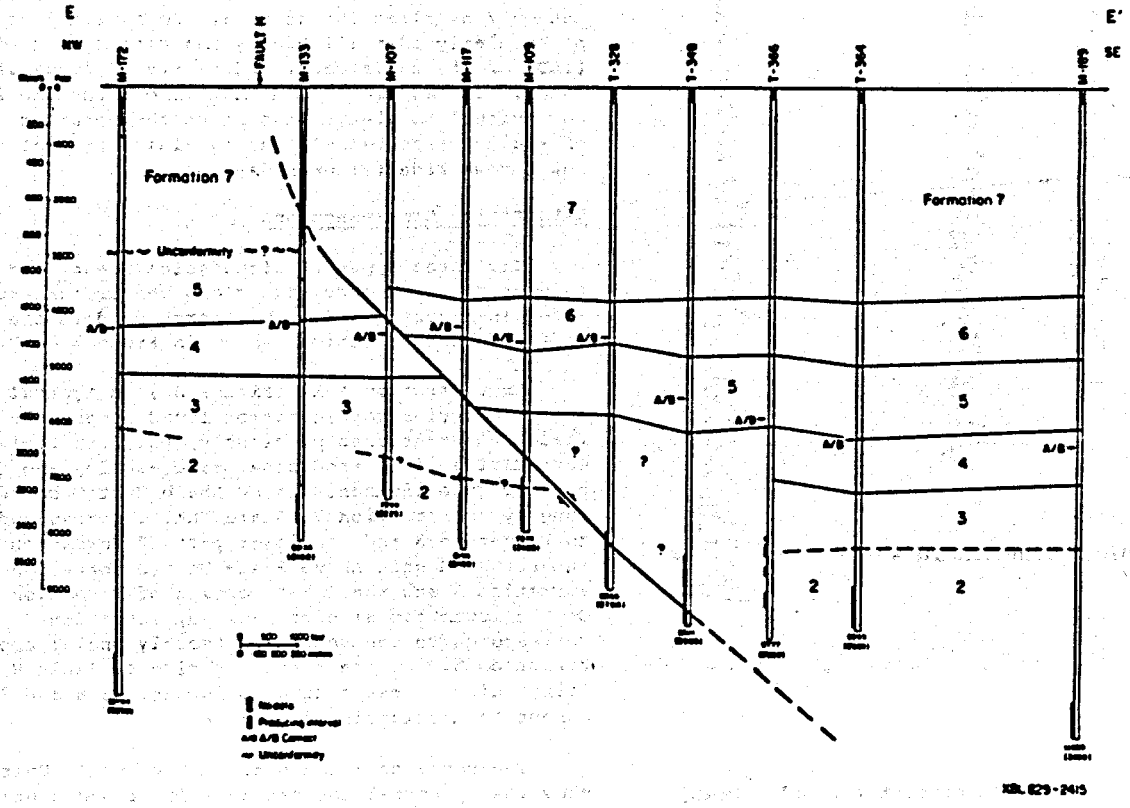

Figure 6E. Formation cross-section E-E'.

West of the railroad tracks, most of the wells have been drilled as deep as Formation 3. The boundary between Formations 3 and 4 is sometimes difficult to define in this region because of the lack of GR logs, which are the easiest to correlate. In this region, geothermal fluid production comes mainly from the A (or α) reservoir (Prian, 1981; Sánchez and de la Peña, 1981), which is located in Formation 4 and in some places extends as much as 500 ft into the upper portion of Formation 3. The temperature of this reservoir ranges from 150°C to 325°C.

The A/B contact, shown in Figure 6A and subsequent figures as "A/B," is the contact between the unconsolidated and consolidated sediments as determined from well cuttings (Puente and de la Peña, 1978). The unconsolidated sediments (Unit A) consist of clays, silts, sands, and gravels. Below this, the consolidated sediments (Unit B) consist of shales, siltstones, and sandstones, some of which are partly metamorphosed.

Previously, some researchers have used the A/B contact as a correlation marker (e.g., Puente and de la Peña, 1978). According to our well log study, however, the A/B contact does not appear to be associated with a correlatable bed. This is illustrated in Figure 7 by the GR logs from wells M-25, E-3, and M-110. For example, the A/B contact for M-25 is located in a shale bed at a depth of 2625 ft, near the top of Formation 5. If the A/B contact were a correlatable marker, it would be associated with this shale bed throughout the field, as shown in Figure 7 by the line labeled A/B. In well E-3, however, the A/B contact is found not in this shale bed but at a much shallower depth (denoted by A/B') within a different unit, at a depth of 1948 ft in Formation 7. Similarly, the A/B contact identified in well M-110 does not correspond to the shale bed of well M-25, but is much deeper (indicated by A/B"), at 3652 ft near the bottom of Formation 5. Thus the A/B contact is not associated with correlatable beds and should not be used as a marker bed.

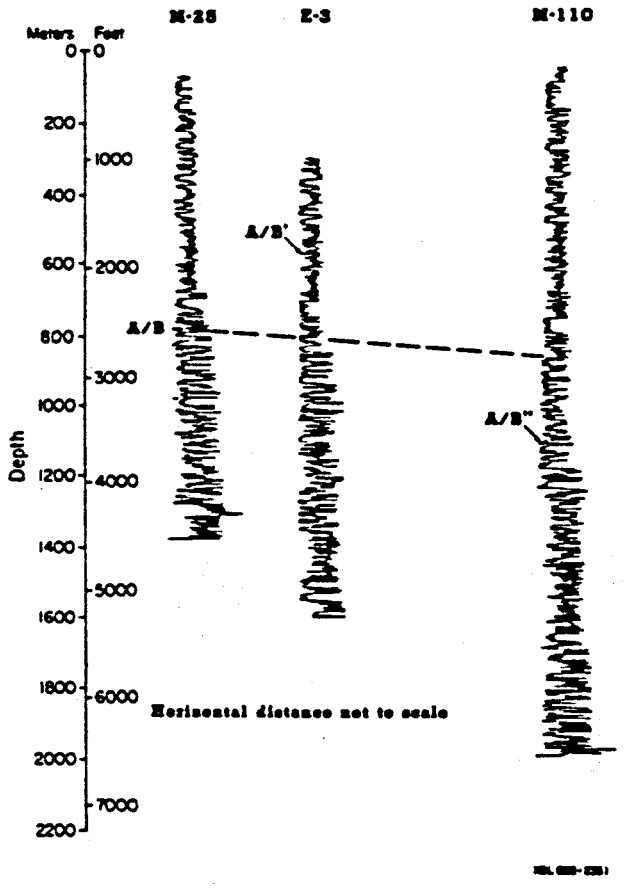

Figure 7. Depths of A/B contact for wells M-25, E-3, and M-110. The traces correspond to gamma-ray logs.

Elders et al. (1978) suggested that the transition from the A and B units is due to induration of the B unit caused by post-depositional events (compaction, cementation, and metamorphic reactions). Seamount and Elders (1981) showed that the depth of first occurrence of thermally altered minerals is generally found near the A/B contact. Later in this paper, we will show that this contact is associated with sharp temperature increases, confirming that it is temperature related. In other words, the heat of the geothermal fluids has caused the induration of the sediments of unit B. On the other hand, the sediments of unit A have remained relatively unaffected except perhaps near their base.

An unconformity has been detected, as indicated in Figures 6A, C-E. For example, in Figure 6A, between wells M-9 and M-150, Formation 7 rests directly on Formation 5 (i.e., Formation 6 is missing), but between Fault H and well NL-1, Formation 7 overlies Formation 6. Formation 6 is particularly identifiable by the high resistivities (ILD) of its sandstones, indicative of freshwater sands. It has been found that throughout the field, Formation 6 is always missing on the upthrown side of Fault H (see below), but is always present on the downthrown side (Figures 6A-E).

Lithofacies Cross-Sections

The three types of lithofacies identified in this study were correlated along the cross-sections shown in Figures 8A-E. They correspond to the formation cross-sections shown in Figures 6A-E.

Cross-section A-A' (Figure 8A) is typical of the lithofacies configuration found across the field. As mentioned previously, the lithofacies were divided into sandstone, sandy-shale, and shale groups. The sediments below Shale Unit O correspond roughly to Formation 2; Shale Unit O corresponds to Formation 3 and the lower part of Formation 4; and the sand unit above Shale Unit O correspond to Formation 5 and the upper portion of Formation 4. On the southwest side of Fault H, Formation 7 corresponds to the sediments (mostly shale) above Formation 5. On the northeast side of Fault H, the lithofacies corresponding to Formations 6 and 7 cannot be distinguished as clearly.

The sandstones and shales above Shale Unit O show fairly normal log readings for a sedimentary environment. Shale Unit O and the sand unit below it show some anomalous log values because they

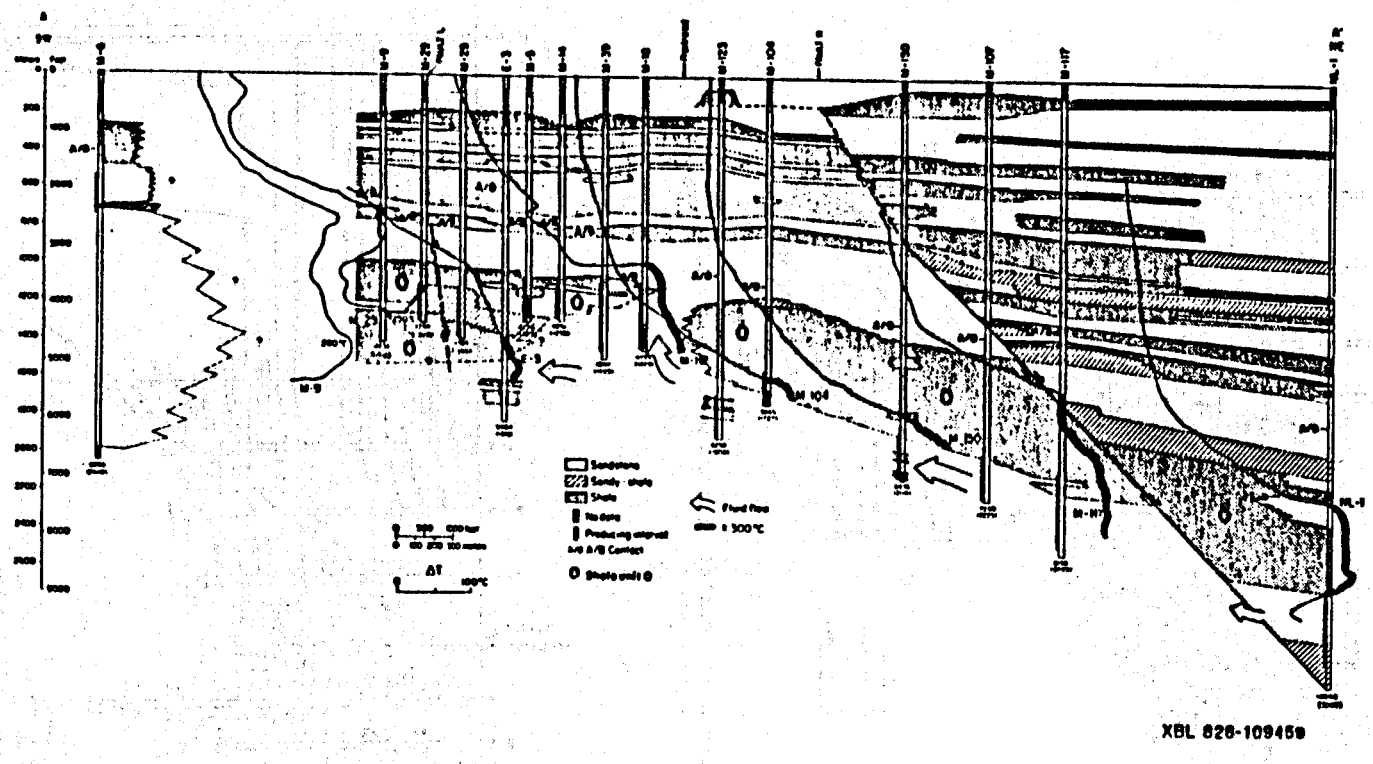

Figure 8A. Lithofacies cross-section A-A'.

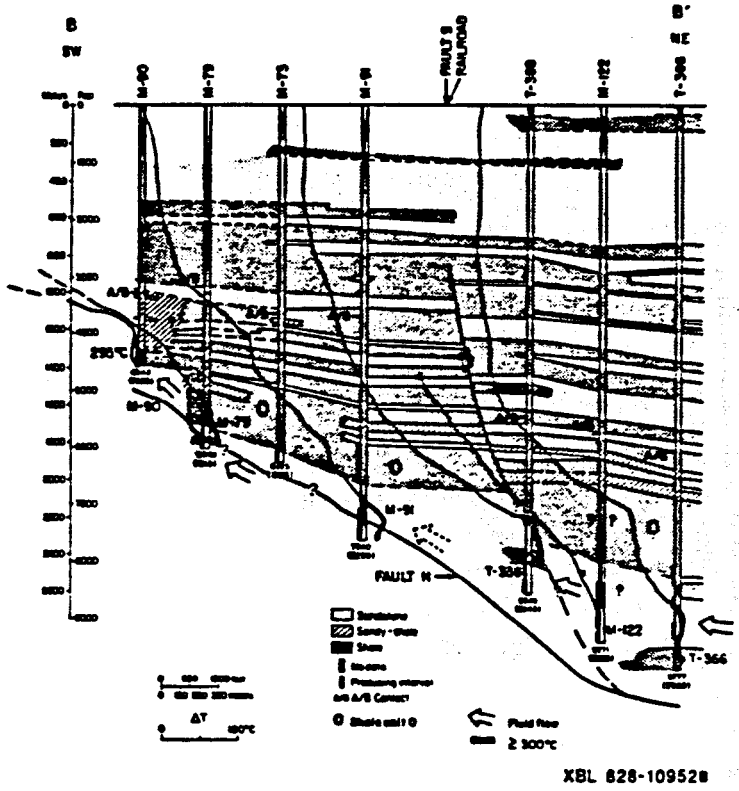

Figure 8B. Lithofacies cross-section B-B'.

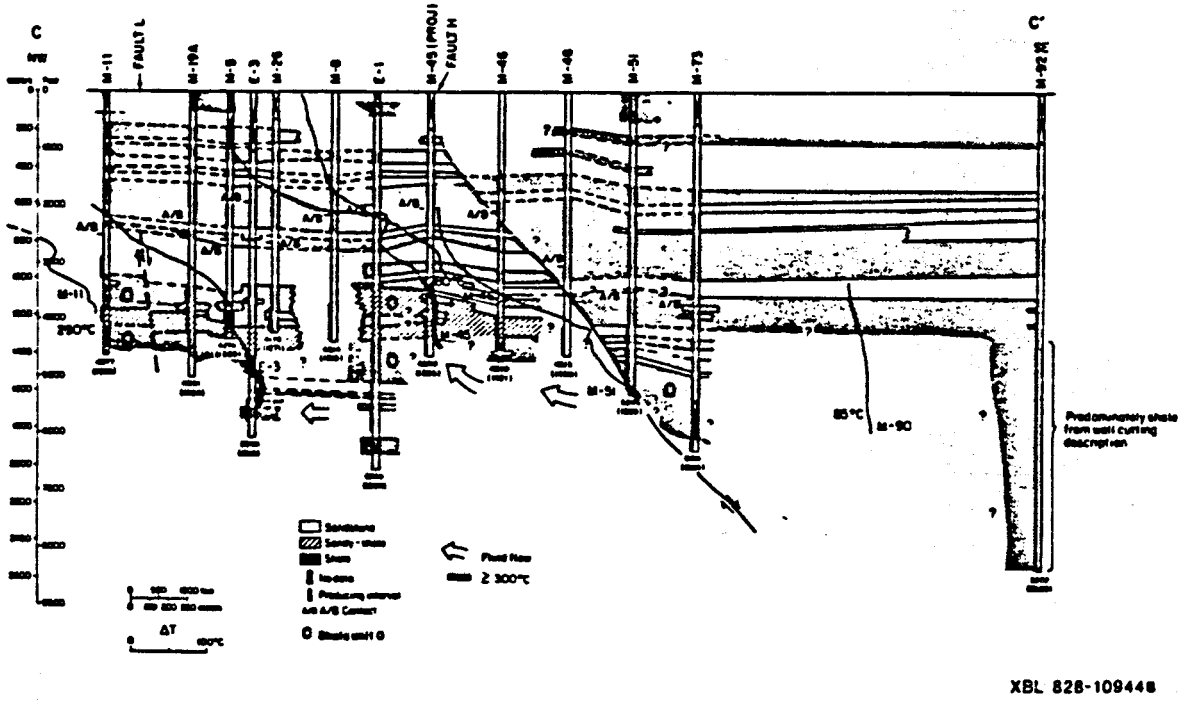

Figure 8C. Lithofacies cross-section C-C'.

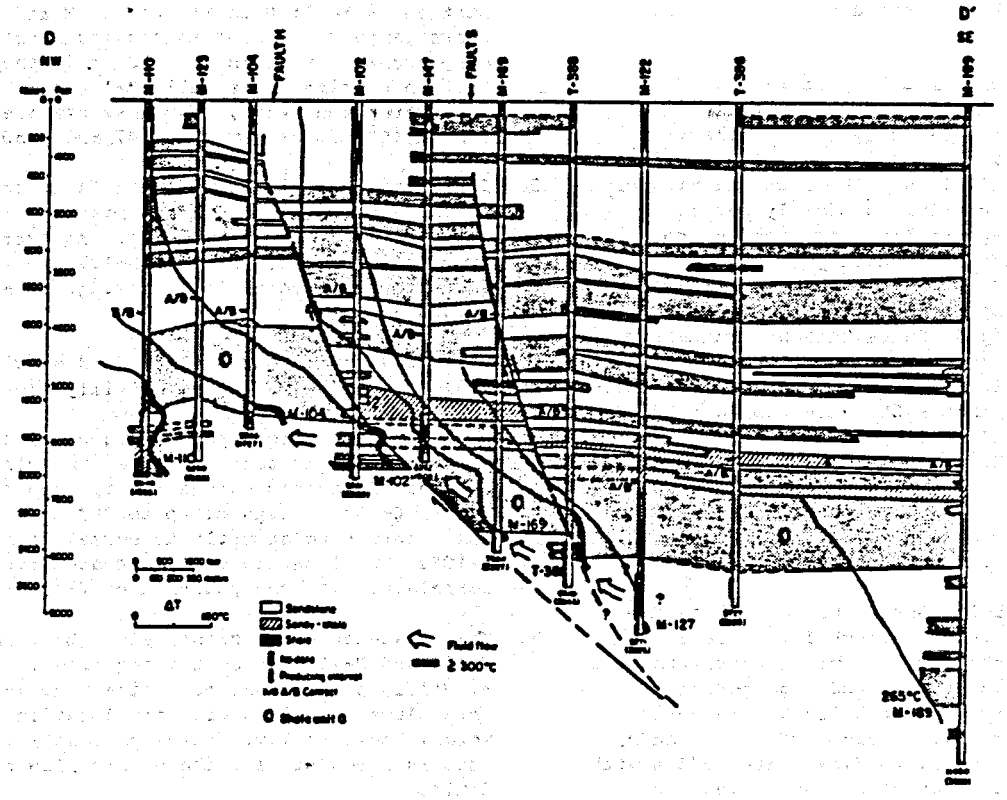

Figure 8D. Lithofacies cross-section D-D'.

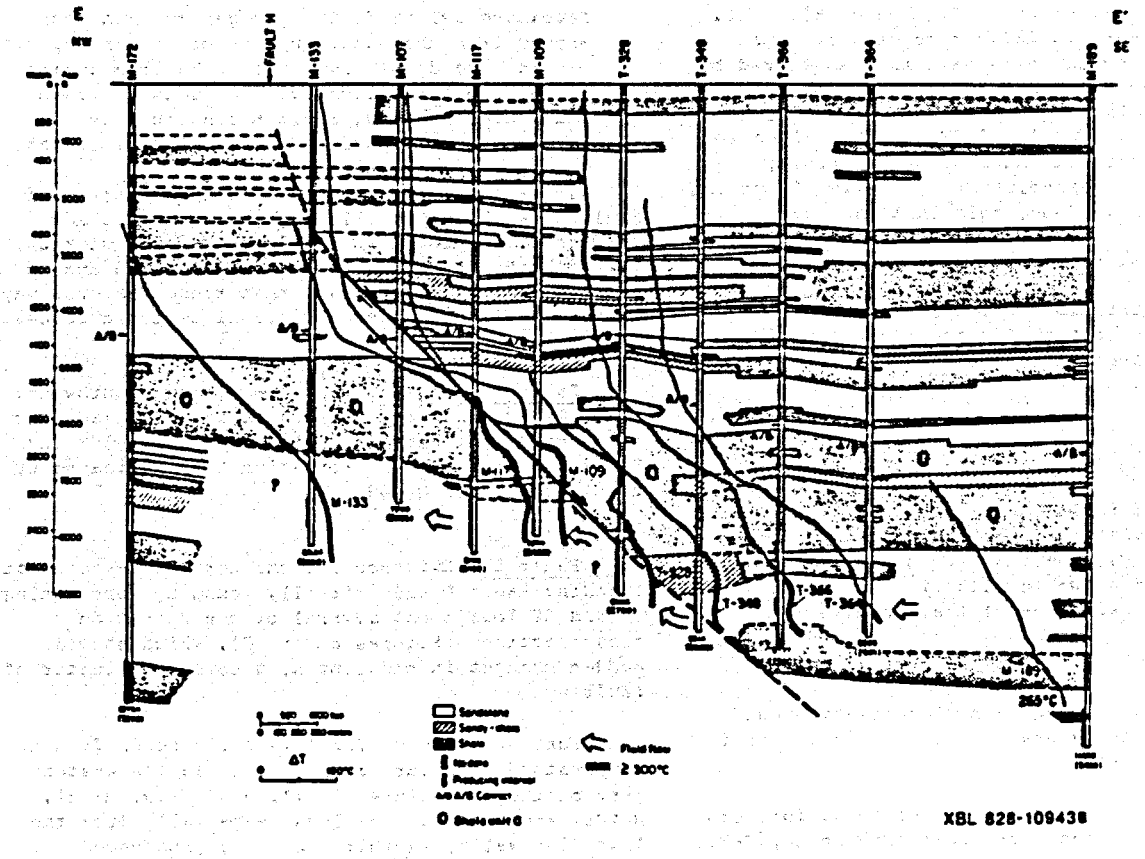

Figure 8E. Lithofacies cross-section E-E'.

have been affected by the circulation of geothermal fluids.

Shale Unit O acts as a barrier to upward migration of geothermal fluid and convective heat flow. This is substantiated by the lithology, thermal characteristics, and low porosity readings obtained from the well logs. The lower portion of Shale Unit O consists mainly of thinly bedded sandstones/ shales (generally corresponding to Formation 3) and lacks any thick permeable sand unit that would permit fluid flow. This is confirmed by the sharp rise in temperature gradient observed near the top of Shale Unit O, indicative of a region where heat is transferred by conduction rather than convection (i.e., fluid flow). Furthermore, the unusually high RHOB values found commonly near the base of Shale Unit O, especially in wells southeast of Fault H, indicate low porosity. This low porosity may be due to induration caused by mineral precipitation (Seamount and Elders, 1981). Thus, the Shale Unit O is a thick, impermeable, low-porosity unit that acts as a (local) cap rock.

The sand unit below Shale Unit O permits the flow of geothermal fluids through it. This is substantiated by lithology, thermal characteristics, depth of producing intervals, and high porosity readings obtained from the well logs. The upper portion of this sand unit consists of thick sands, conducive to permitting fluid flow, interbedded with some shales (generally corresponding to the upper portion of Formation 2). In this unit, the temperature profiles show a fairly constant temperature of 300°C or slightly greater (temperatures greater than 300°C are indicated by the heavier lines in the temperature profiles shown in Figures 8A-E). This constant temperature is indicative of circulating fluids, i.e., a region where heat is transferred by convection rather than conduction. Most of the producing intervals for the β reservoir are located in this sand unit. The low ILD and RHOB values for the sand beds within it indicate high porosity, possibly secondary (dissolution) porosity (Lyons and van de Kamp, 1980). Thus, this unit has thick, permeable, high porosity sands and acts as a conduit for the geothermal fluid.

Further description of the lithofacies and the role they play in controlling the flow of geothermal fluids will be given in the section on Geothermal Fluid Flow Paths.

Faults

Three buried faults have been identified in this study as having an important impact on geothermal fluid flow. They have been named Faults H, L, and S, and are shown in plan view in Figure 1. Evidence for the existence of these faults is described below.

Fault H. Fault H has a northeast-southwest strike. Its existence was established on the basis of several evidences.

1. A large vertical displacement of formations can be correlated across the fault (Figure 6A, C-E). The lower portion of the fault (solid line portion of Fault H in Figures 6A-E and 8A-E) shows large downthrows to the southeast, with displacements as much as 1650 ft in the northeastern portion (near wells M-150 and M-107). Toward the southwest, displacements are smaller (about 1000 ft near wells M-47 and M-50).

2. Logs from wells located in the fault zone have portions or whole formations missing, which is indicative of normal faulting. An example of this is illustrated by well M-107, in which Formation 5 is completely missing, as shown in Figure 6A.

3. Seismic sections across the field show that Fault H exists (Majer and McEvilly, 1982).

4. The only available dipmeter log covering the postulated fault zone (obtained in well M-107) indicates a sudden change in dip from the normal 0-10° to dips of up to 30° over a 200-ft span, returning abruptly to normal dips of 0-10°. The location of this sudden dip change correlates with the position of Fault H.

5. The existence of a thermal plume between wells M-109 and M-107 has been recognized by A. Williams (personal communication, 1982). This plume coincides with the location of Fault H, which, incidentally, indicates that this fault acts as a conduit for the upward flow of hot fluid.

6. The absence of Formation 6 on the upthrown side of Fault H is related to the movement of this fault (Figures 6A, C-E). Either Formation 6 was deposited before faulting began and was then eroded from the upthrown side or it was deposited only on the downthrown side of Fault H as (or after) faulting occurred. The logs indicate that movement along Fault H continued as the sediments of Formation 7 were being deposited.

It is interesting to note that the strike of Fault H is almost parallel to that of dikes and surface faults found at the Cerro Prieto volcano. west of the geothermal field (Alonso, 1966 and de Boer, 1979). This suggests that these features may be the result of the same regional tectonic forces.

Fault S. Fault S trends northeast-southwest. The only evidence for this fault is a displacement of about 400 ft between wells M-169 and T-388 and the absence of part of Formation 6 as indicated by the logs of well M-169.

Fault L. Evidence for the northeast-southwest-trending Fault L was initially found by correlating GR and SP logs along several of the formation cross-sections (Figures 6A and C), which showed sudden changes in bed depths, a common indicator of faulting.

Further evidence for this fault comes from the temperature logs for several wells in the western part of the field (M-43, M-11, M-9, M-29, M-181, M-105, and O-473). The logs, especially from the last five wells, exhibit unusually pronounced temperature reversals (e.g., see Figures 8A and C),

which reflect the presence of aquifers of different temperatures.

GEOTHERMAL FLUID FLOW PATHS

The model showing the movement of geothermal fluids in the Cerro Prieto system was obtained by analyzing the available data pertaining to the sections shown in Figures 8A-E and was selected to represent the whole field. Following the method outlined by Howard (1981), we found that the actual fluid flow paths become readily apparent when downhole temperature profiles (Bermejo et al., 1979; personal communication, 1982) and well production intervals were superimposed on the lithofacies sections (Figures 8A-E). The various sections and the suggested fluid flow paths across them are discussed below.

Cross-section A-A'

Figure 8A shows the lithofacies cross-section A-A', on which temperature profiles, A/B contacts (Cobo R., 1981), and production intervals were superimposed. The parts of the temperature profiles shown by heavy lines indicate temperatures of 300°C or greater. The maximum temperatures of cooler wells are indicated next to the corresponding curve.

From Figure 8A it can be seen that the logs show sharp temperature increases near the A/B contact and that the A/B contact, the producing intervals, and the sharp increases in temperature are observed at progressively greater depths toward the east. Well M-117 does not conform to this trend, however, and will be discussed below.

Comparison of the temperature profiles with the lithology (Figure 8A) of wells M-104, M-150, and NL-1 indicates that sharp increases in temperature gradient occur near the boundary between Shale Unit O and the overlying sand unit. In wells E-3, M-29, and M-9, this temperature increase is observed near another shale bed, which occurs in well M-29 at the same depth as the A/B contact. The increase in temperature, therefore, suggests that the shale units must be barriers to convective heat transport; i.e., they are essentially acting as local cap rocks.

According to W. Elders (personal communication, 1982), the heat source for the Cerro Prieto system is associated with a swarm of dikes intruded in the eastern regions of the field. These rocks heat the circulating fluid which is thought to enter the field from the east through the sand underlying Shale Unit O, after which it moves westward toward Fault H (arrows in Figure 8A indicate the direction of the fluid flow path). The fluid then flows up Fault H until it encounters the bottom of the Shale Unit O once again. A small portion of the fluid continues up Fault H, resulting in a temperature of 300°C at a shallow depth in well M-117. Most of the fluid, however, moves westward into the sand below the upthrown Shale Unit O. This flow continues until it reaches a sandy gap in Shale Unit O, in the general area of well M-10. There, the geothermal fluid flows upward into this gap, resulting in high temperatures in well M-10 at shallow depths. Some of the fluid enters the southwestern part of Shale Unit O, which is sandier than in the east, and moves westward until encountering Fault L. There, the fluid flows upward through this fault and then westward through the sands above Shale Unit O. Fluid that does not enter Shale Unit O continues to flow westward through the sands under Shale Unit O. Eventually, some fluid leaks to the surface through the Cerro Prieto Fault Zone, which bounds the field to the west (see Figure 1), and the rest mixes with the colder waters that surround the geothermal anomaly.

Throughout the field, the β reservoir is located in the sands beneath Shale Unit O. The α reservoir is restricted to the western portion of Shale Unit O, west of the railroad tracks. The geothermal fluid flowing westward through the β reservoir is also able to flow into the α reservoir through the sandy gap in the vicinity of well M-10. Thus our model indicates that the two reservoirs are interconnected, contrary to what was postulated by Prian (1981) and Sánchez and de la Peña (1981).

Cross-sections E-E', D-D', C-C', and B-B'

A similar pattern of fluid flow can be seen in cross-section E-E'. Most of the fluid appears to flow from east to west through the sand under Shale Unit O, then up Fault H until it once again encounters the base of Shale Unit O. A portion of the fluid continues flowing up the fault, as indicated by shallower 300°C isotherms and A/B contacts in wells M-107, M-117, M-109, and T-328. However, most of the fluid moves westward through the sands below Shale Unit O (β reservoir).

Cross-sections C-C' and D-D' show basically the same fluid flow patterns as shown in cross-sections A-A' and E-E'.

Cross-section B-B' is somewhat parallel to the strike of Fault H (Figure 5). However, the fluid flow pattern is similar.

Most of the geothermal fluid is believed to flow through a high-porosity, permeable sand underlying the low-porosity, impermeable Shale Unit O, which acts as a local cap rock. Figure 9 shows a contour map of the top of this sand, which corresponds to the top of the β reservoir. The postulated direction of geothermal fluid flow through these sands is indicated by the arrows. As indicated by this figure, the fluid is generally believed to enter the field (at great depth) from the east, gradually moving westward (and rising to shallower depths), and finally leaking to the surface in the western regions of the field. Several wells to the east are cooler (i.e., M-189 in Figures 8D and E, and M-92 in Figure 8C). This suggests that these wells are bypassed by the hot fluids entering the field from the east, north of these wells.

SUMMARY AND CONCLUSIONS

By integrating the geologic model of Cerro Prieto with downhole temperature profiles and well production intervals, the geothermal fluid flow paths in the field have been identified. Based on the information obtained from all the wells, the hot

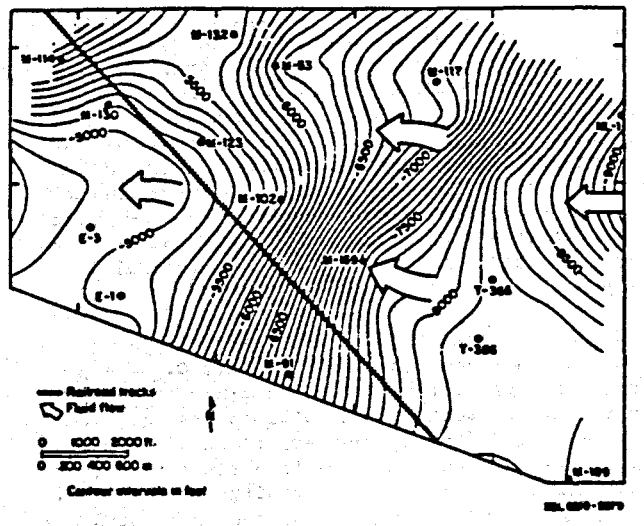

Figure 9. Contour lines indicate the top of the β reservoir. Arrows indicate the direction of geothermal fluid flow.

geothermal fluids appear to be entering the field at depth from the southeast through permeable sands below Shale Unit O, which is acting as a local cap rock. These fluids flow toward and up Fault H until they encounter the same permeable sands below Shale Unit O on the upthrown side of this fault, where they continue to move in a westward direction. When the fluid encounters a break in the shales, some fluid ascends once again to enter the sandier western part of Shale Unit O, where the α reservoir is located, and the rest continues flowing westward through the sand below Shale Unit O (β reservoir). Eventually, some of the geothermal fluid reaches the surface in the western region of the field; the rest mixes with cooler groundwaters.

This work is consistent with mineralogical (Elders et al., 1981), thermal (Mercado, 1976), reservoir engineering, and geochemical (Grant et al., 1981) studies carried out in this geothermal system. Our results form the basis for numerical modeling of the behavior of the Cerro Prieto field in its natural state and under exploitation (Lippmann and Bodvarsson, 1982; Tsang et al., 1982).

ACKNOWLEDGEMENTS

We would like to thank our colleagues of the Comisión Federal de Electricidad for providing all the data used in this study. We are indebted to Marilee Bailey, for the many hours she spent drafting the illustrations, and to Mark Sluka and Lynn Goettinger, who patiently digitized the well logs. Special thanks go to Aylette Villemain, who spent many late evenings revising and typing the early versions of this manuscript.

This work was supported by the Assistant Secretary for Conservation and Renewable Energy, Office of Renewable Technology, Division of Geothermal and Hydropower Technologies of the U.S. Department of Energy under contract No. DE-AC03-76SF00098.

REFERENCES

Alonso E., H., 1966. La zona geotérmica de Cerro Prieto, Baja California, Bol. Sociedad Geológica Mexicana, v. 29, pp. 17-47.

Bermejo M., F.J., Navarro O., F.X., Castillo B., F., Esquer, C.A., and Cortez A., C., 1979. Pressure variations at the Cerro Prieto reservoir during production, in Proceedings, Second Symposium on the Cerro Prieto geothermal field, October 17-19, 1979. Mexicali, Comisión Federal de Electricidad, pp. 473-493.

Cobo R., J.M., 1981. Configuration of mudstones, gray- and coffee-colored shale lithologic units, zones of silica and epidote, and their relationship to the tectonics of the Cerro Prieto geothermal field, in Proceedings, Third Symposium on the Cerro Prieto geothermal field, September 20-22, 1981. Berkeley, Lawrence Berkeley Laboratory report LBL-7098, pp. 29-42.

de Boer, J., 1979. Paleomagnetism of the Quaternary Cerro Prieto, Crater Elegante, and Salton Buttes Volcanic Domes in the northern part of the Gulf of California rhombochaom, in Proceedings, Second Symposium on the Cerro Prieto geothermal field, October 17-19, 1979. Mexicali, Comisión Federal de Electricidad, pp. 91-98.

Elders, W.A., Hoagland, J.R., McDowell, S.D., and Cobo R.J.M., 1978. Hydrothermal mineral zones in the geothermal reservoir of Cerro Prieto, in Proceedings, First Symposium on the Cerro Prieto geothermal field, September 20-22, 1978. Berkeley, Lawrence Berkeley Laboratory Report LBL-7098, pp. 68-75.

Elders, W.A., Williams A.E., and Hoagland, J.R., 1981. An integrated model for the natural flow regime in the Cerro Prieto hydrothermal system based upon petrological and isotope geochemical data, in Proceedings, Third Symposium on the Cerro Prieto geothermal field, March 24-26, 1981. Berkeley, Lawrence Berkeley Laboratory Report LBL-11967, pp. 102-109.

Grant, M.A., Truesdell, A.H., and Mañón M., A., 1981. Production induced boiling and cold water entry in the Cerro Prieto Geothermal reservoir indicated by chemical and physical measurements, in Proceedings, Third Symposium on the Cerro Prieto geothermal field, March 24-26, 1981. Berkeley, Lawrence Berkeley Laboratory, LBL-11967, pp. 274-280, pp. 221-237.

Howard, J.H., 1981. Comments on the geology of the Cerro Prieto geothermal field as of the AAPG meeting 1981, Berkeley, Lawrence Berkeley Laboratory Internal Memorandum.

Lippmann, M.J., and Bodvarsson, G.S., 1982. Modeling studies on Cerro Prieto, in Proceedings, Fourth Symposium on the Cerro Prieto geothermal field, this volume.

Lyons, D.J., and van de Kamp, P.C., 1980. Subsurface geological and geophysical study of the Cerro Prieto geothermal field, Baja California, Mexico. Berkeley, Lawrence Berkeley Laboratory Report LBL-10540.

Majer, E.L., and McEvilly, T.V., 1982. Seismological studies at the Cerro Prieto field: 1978-1982, in Proceedings, Fourth Symposium on the Cerro Prieto geothermal field, this volume.

Mercado G., S., 1968. Localización de zonas de máxima actividad hidrotermal por medio de proporciones químicas, campo geotérmico de Cerro Prieto, B.C. Presented at the III Congreso Mexicano de Química Pura y Aplicada, March 21-23, 1968. Guadalajara, México: Sociedad Química de México.

Mercado G., S., 1976. Movement of geothermal fluids and temperature distribution in the Cerro Prieto geothermal field, in Proceedings, Second United Nations Symposium on the Development and Use of Geothermal Resources, San Francisco, California, May 20-29, 1975, pp. 489-494.

Prian C., R., 1981. Velocidad de perforación de la secuencia estratigráfica del área de Cerro Prieto, in Proceedings, Third Symposium on the Cerro Prieto geothermal field, March 24-26, 1981. Berkeley, Lawrence Berkeley Laboratory Report LBL-11967, pp. 77-85.

Puente C., I., and de la Peña L., A., 1978. Geology of the Cerro Prieto geothermal field, in Proceedings, First Symposium on the Cerro Prieto Geothermal field, September 20-22, 1978. Berkeley, Lawrence Berkeley Laboratory Report LBL-7098, pp. 17-37.

Sánchez R., J., and de la Peña L., A., 1978. Geohydrology of the Cerro Prieto geothermal aquifer, in Proceedings, Third Symposium on the Cerro Prieto geothermal field, March 24-26, 1981. Berkeley, Lawrence Berkeley Laboratory Report LBL-11967, pp. 309-323.

Seamount, D.T., and Elders, W.A., 1981. Use of wireline logs at Cerro Prieto in identification of the distribution of hydrothermally altered zones and dike locations, and their correlation with reservoir temperatures, in Proceedings, Third Symposium on the Cerro Prieto geothermal field, March 24-26, 1981. Berkeley, Lawrence Berkeley Laboratory Report LBL-11967, pp.123-133.

Tsang, C.F., Mangold, D.C., Doughty, C., and Lippmann, M.J., 1982. Prediction of reinjection effects in the Cerro Prieto geothermal system, in Proceedings, Fourth Symposium on the Cerro Prieto geothermal field, this volume.